Theses and Dissertations          1. Thesis and Dissertation Collection, all items

2016-12

# Integrated heat exchange for recuperation in gas turbine engines

## Hussein, Faisa T.

Monterey, California: Naval Postgraduate School

http://hdl.handle.net/10945/51722

http://www.nps.edu/library

# NAVAL POSTGRADUATE SCHOOL

## MONTEREY, CALIFORNIA

# THESIS

**INTEGRATED HEAT EXCHANGE FOR RECUPERATION IN GAS TURBINE ENGINES**

by

Faisa T. Hussein

December 2016

| | |
|---|---|
| Thesis Advisor: | Anthony J. Gannon |
| Co-Advisor: | Garth V. Hobson |

**Approved for public release. Distribution is unlimited.**

THIS PAGE INTENTIONALLY LEFT BLANK

| REPORT DOCUMENTATION PAGE | | *Form Approved OMB No. 0704–0188* |
|---|---|---|

Public reporting burden for this collection of information is estimated to average 1 hour per response, including the time for reviewing instruction, searching existing data sources, gathering and maintaining the data needed, and completing and reviewing the collection of information. Send comments regarding this burden estimate or any other aspect of this collection of information, including suggestions for reducing this burden, to Washington headquarters Services, Directorate for Information Operations and Reports, 1215 Jefferson Davis Highway, Suite 1204, Arlington, VA 22202-4302, and to the Office of Management and Budget, Paperwork Reduction Project (0704-0188) Washington, DC 20503.

| 1. AGENCY USE ONLY (*Leave blank*) | 2. REPORT DATE December 2016 | 3. REPORT TYPE AND DATES COVERED Master's thesis | |
|---|---|---|---|
| **4. TITLE AND SUBTITLE** INTEGRATED HEAT EXCHANGE FOR RECUPERATION IN GAS TURBINE ENGINES | | **5. FUNDING NUMBERS** | |
| **6. AUTHOR(S)** Faisa T. Hussein | | | |
| **7. PERFORMING ORGANIZATION NAME(S) AND ADDRESS(ES)** Naval Postgraduate School Monterey, CA 93943-5000 | | **8. PERFORMING ORGANIZATION REPORT NUMBER** | |
| **9. SPONSORING /MONITORING AGENCY NAME(S) AND ADDRESS(ES)** N/A | | **10. SPONSORING / MONITORING AGENCY REPORT NUMBER** | |

**11. SUPPLEMENTARY NOTES** The views expressed in this thesis are those of the author and do not reflect the official policy or position of the Department of Defense or the U.S. Government. IRB Protocol number _____N/A_____.

| 12a. DISTRIBUTION / AVAILABILITY STATEMENT Approved for public release. Distribution is unlimited. | 12b. DISTRIBUTION CODE |
|---|---|

**13. ABSTRACT (maximum 200 words)**

While the use of recuperators in gas turbine engines is quite favorable for increasing cycle efficiency, it is currently only feasible to apply this technology to land-based engines. Transferring this technology to aviation or ship gas turbines is difficult due the size and weight of the heat exchanger components required. An alternate approach would be to embed a heat exchange system within the engine using existing blade surfaces to extract and insert heat. Due to the highly turbulent and transient flow, heat transfer coefficients in turbomachinery are extremely high, making this possible. Heat transfer between the turbine and compressor blade surfaces could be accomplished using evaporative heat pipes.

This study explores the feasibility of embedding this heat exchange system within engines using a thermodynamic approach to quantify cycle improvements and compare them to those of other modified cycles. The real performance effects are taken into account based on the heat transfer coefficients within turbomachinery obtained from experimental studies.

The effectiveness of an integrated heat exchange system was found to be 4.5%. Using this integrated heat exchange system for recuperation in gas turbine cycles improves efficiency at pressure ratios less than 22. Using this heat exchange system for intercooling improves efficiency from 1% to 2% and increases engine power output by 1% to 7%, depending on pressure ratio. Cycle improvements of over 1% in efficiency can lead to significant fuel savings for both the USN and USMC.

| 14. SUBJECT TERMS heat transfer, recuperation, regeneration, gas turbine, heat pipe, cycle improvements | | | 15. NUMBER OF PAGES 67 |
|---|---|---|---|
| | | | 16. PRICE CODE |
| 17. SECURITY CLASSIFICATION OF REPORT Unclassified | 18. SECURITY CLASSIFICATION OF THIS PAGE Unclassified | 19. SECURITY CLASSIFICATION OF ABSTRACT Unclassified | 20. LIMITATION OF ABSTRACT UU |

THIS PAGE INTENTIONALLY LEFT BLANK

**INTEGRATED HEAT EXCHANGE FOR RECUPERATION IN GAS TURBINE
ENGINES**

Faisa T. Hussein
Lieutenant, United States Navy
B.S., University of Notre Dame, 2011

Submitted in partial fulfillment of the
requirements for the degree of

**MASTER OF SCIENCE IN MECHANICAL ENGINEERING**

from the

**NAVAL POSTGRADUATE SCHOOL
December 2016**

Approved by:        Dr. Anthony Gannon
                    Thesis Advisor

                    Dr. Garth Hobson
                    Co-Advisor

                    Dr. Garth Hobson
                    Chair, Department of Mechanical and Aerospace Engineering

THIS PAGE INTENTIONALLY LEFT BLANK

# ABSTRACT

While the use of recuperators in gas turbine engines is quite favorable for increasing cycle efficiency, it is currently only feasible to apply this technology to land-based engines. Transferring this technology to aviation or ship gas turbines is difficult due the size and weight of the heat exchanger components required. An alternate approach would be to embed a heat exchange system within the engine using existing blade surfaces to extract and insert heat. Due to the highly turbulent and transient flow, heat transfer coefficients in turbomachinery are extremely high, making this possible. Heat transfer between the turbine and compressor blade surfaces could be accomplished using evaporative heat pipes.

This study explores the feasibility of embedding this heat exchange system within engines using a thermodynamic approach to quantify cycle improvements and compare them to those of other modified cycles. The real performance effects are taken into account based on the heat transfer coefficients within turbomachinery obtained from experimental studies.

The effectiveness of an integrated heat exchange system was found to be 4.5%. Using this integrated heat exchange system for recuperation in gas turbine cycles improves efficiency at pressure ratios less than 22. Using this heat exchange system for intercooling improves efficiency from 1% to 2% and increases engine power output by 1% to 7%, depending on pressure ratio. Cycle improvements of over 1% in efficiency can lead to significant fuel savings for both the USN and USMC.

THIS PAGE INTENTIONALLY LEFT BLANK

# TABLE OF CONTENTS

# LIST OF FIGURES

THIS PAGE INTENTIONALLY LEFT BLANK

# LIST OF TABLES

THIS PAGE INTENTIONALLY LEFT BLANK

# LIST OF ACRONYMS AND ABBREVIATIONS

| | |
|---|---|
| CFD | Computational Fluid Dynamics |
| CPU | Central Processing Unit |
| DON | Department of the Navy |
| IR | Infrared |
| NASA | National Aeronautics and Space Administration |
| NTU | Number of Transfer Units |
| Nu | Nusselt Number |
| PT | Total Pressure |
| TT | Total Temperature |
| T-S | Temperature-Entropy |

THIS PAGE INTENTIONALLY LEFT BLANK

# NOMENCLATURE

| Symbol | Description | Units |
|--------|-------------|-------|
| $A_b$ | Blade area | [m$^2$] |
| $A_c$ | Cold section area | [m$^2$] |
| $A_{case}$ | Casing area | [m$^2$] |
| $A_f$ | Frontal Area | [m$^2$] |
| $A_h$ | Hot section area | [m$^2$] |
| $A_{hub}$ | Hub area | [m$^2$] |
| $A_{tot}$ | Total area | [m$^2$] |
| $C$ | Heat capacity rate | [W/K] |
| $C_p$ | Specific heat (const. P) | [J-kg/K] |
| $c$ | Chord | [m] |
| $D_i$ | Inner diameter | [m] |
| $D_o$ | Outer diameter | [m] |
| $D_h$ | Hydraulic diameter | [m] |
| $g$ | Gravitational Constant | [m/s$^2$] |
| $h$ | Enthalpy, heat transfer coefficient | [J], [W/m$^2$-K] |
| $k$ | Thermal conductivity | [W/m-K] |
| $l$ | Blade height | [m] |
| $\dot{m}$ | Mass flowrate | [kg/s] |

| Symbol | Description | Units |
|--------|-------------|-------|
| $Nu$ | Nusselt Number | - |
| $NTU$ | Number of Transfer Units | - |
| $n$ | Number of blades | - |
| $P$ | Pressure, Perimeter | $[N/m^2]$, $[m]$ |
| $Q$ | Heat transfer | $[J]$ |
| $q$ | Heat transfer rate | $[W]$ |
| $s$ | Spacing | $[m]$ |
| $T$ | Temperature | $[K]$ |
| $U$ | Overall heat transfer coefficient | $[W/m^2\text{-}K]$ |
| $V_{ax}$ | Axial velocity | $[m/s]$ |
| $w$ | Work | $[J]$ |
| $x$ | Area ratio | - |
| $Z$ | Height | $[m]$ |

Greek Letters

| | | |
|--------|-------------|-------|
| $\gamma$ | Specific heat ratio | - |
| $\varepsilon$ | Effectiveness | - |
| $\eta$ | Efficiency | - |
| $\nu$ | Velocity | $[m/s]$ |
| $\rho$ | Mass density | $[kg/m^3]$ |
| $\sigma$ | Solidity | - |
| $\phi$ | Aspect Ratio | - |

| Symbol | Description |
|--------|-------------|
| Subscripts | |
| *comp* | Compressor |
| *e* | Exit |
| *i* | Inlet |
| *in* | Input |
| max | Maximum |
| min | Minimum |
| *net* | Net |
| *out* | Output |
| *turb* | Turbine |

THIS PAGE INTENTIONALLY LEFT BLANK

# I. INTRODUCTION

## A. PROBLEM STATEMENT

The U.S. Navy (USN) and U.S. Marine Corps (USMC) rely heavily on gas turbine engines to power and propel vehicles, ships and aircraft. These powerplants have a high power density allowing for enhanced capabilities for USN and USMC ships and aerial platforms; however, fuel and the associated logistical support is critical to every mission, and thus will always present a significant vulnerability. One of the largest obstacles the military faces is its dependence on petroleum-based fuels.

The Secretary of the Navy (SECNAV) has made energy efficiency a priority for the USN and USMC [1]. The "Strategy for Renewable Energy" [1] outlines the SECNAV's five energy goals. The number one goal is to increase the use of alternative energy within the Department of the Navy (DON). Additionally, departmental energy programs have focused heavily on reducing energy demand by improving efficiency. Land-based gas turbine engines commonly use recuperated cycles to increase cycle efficiency. Transferring this technology to aviation and ship engines is difficult due to the size and weight of heat exchanger components.

The aim of this work is to use thermodynamic and heat transfer theory, coupled with new experimental data, to determine whether it is feasible to design an aviation engine with a heat exchange system embedded within the engine using the existing blade surfaces to extract and insert heat.

## B. LITERATURE REVIEW

### 1. Recuperated Gas Turbine

The WR-21 is a gas turbine engine originally designed in an international partnership between Northrop Grumman Marine Systems and Rolls Royce [2]. It has an intercooled recuperator and is currently in use aboard the British Royal Navy's Type 45 destroyers [3]. Figure 1 is a schematic of the WR-21 intercooled recuperated engine.
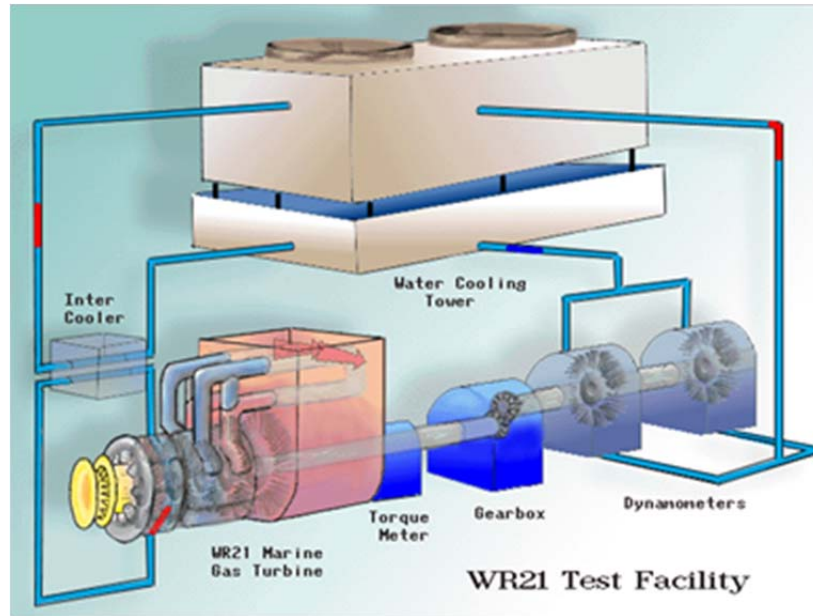
Figure 1.    WR-21 Intercooled Recuperated Gas Turbine. Source: [3].

The intercooler-recuperator recovers what would be waste heat from the exhaust and returns it to the engine.  This makes the gas turbine more fuel-efficient and reduces the ships Infrared Radiation (IR) signature.  There is, however, a significant design flaw in the intercooler, which causes the gas turbine to shut down when the ship is operating in warm water.  When this engine failure occurs the ship is left dead in the water, with no source of propulsion.

## 2.    Steam Cooling in Gas Turbines

The G class steam cooled gas turbine developed by Mitsubishi uses steam cooling in the compressor stator blades.  Not only does steam provide a better heat transfer medium than air, using steam for cooling leaves more air available for combustion. Because steam cooling involves an integrated cooling circuit within the cycle, a back-up steam cooling unit is required in case of an interruption to the steam supply [4].  This involves the addition of multiple engine components which is acceptable, only, for this land-based engine.

### 3.    Heat Transfer in Gas Turbine Compressors

Very few compressor designs take heat transfer into consideration. Most testing and simulation is with the assumption that the compressor end-walls are adiabatic. There has been some exploration into the use of heat transfer to improve the performance and efficiency of an engine cycle.

The effect of blade passage surface heat removal on an axial compressor, in order to precool the front end of a turbomachine, was investigated by Shah and Tan [5]. Using computational fluid dynamics (CFD), Shah and Tan [5] simulated heat removal in a compressor via the blade passage surfaces, a process known as compressor cooling. These simulations were conducted for a one-stage as well as an eight-stage compressor. In both cases, compressor cooling resulted in increased compressor pressure ratios, increased mass flow capability and an increase in the cycle efficiency. These simulations, however, were still performed with the assumption of adiabatic flow through the compressor.

Bruna and Turner [6] performed CFD simulations of the National Aeronautics and Space Administration (NASA) Rotor 37 axial compressor assuming isothermal boundary conditions and compared their results with simulations assuming an adiabatic boundary condition. The temperature profile and efficiency results of the isothermal assumption better matched experimental data than the adiabatic assumption. Considering heat transfer resulted in a 1% higher efficiency than the adiabatic approach, meaning heat transfer accounts for about 1% efficiency.

Researchers at the Naval Postgraduate School have performed an axisymmetric heat transfer analysis in a compressor casing assuming non-adiabatic conditions [7]. The heat transfer was assessed using thermocouples to measure temperatures on the casing outer wall and heat transfer coefficients were determined for 100% and 90% speeds.

Figure 2 is a schematic for the cross-section of the transonic rotor rig used for testing. The casing is aluminum (non-adiabatic) except for an abradable material directly above the rotor used to vary tip gap, which has a very low heat transfer coefficient and can be considered adiabatic [8].
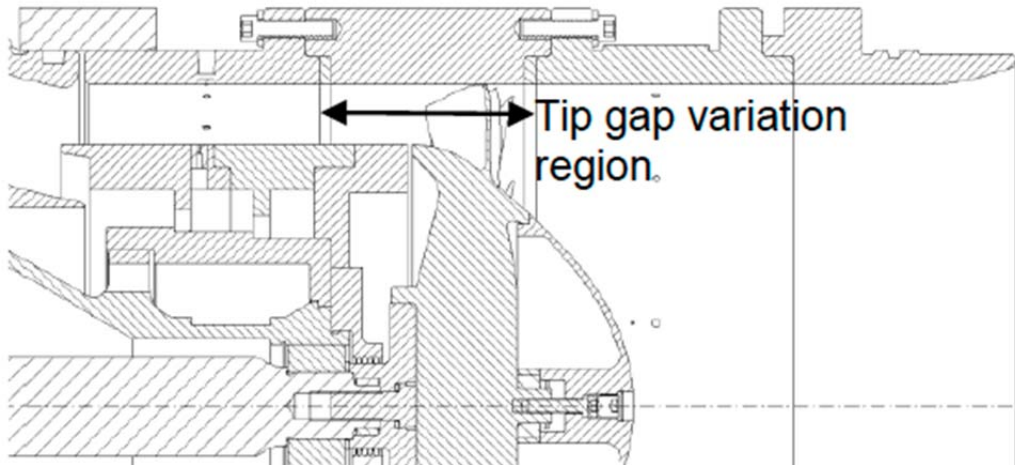
Figure 2.     Transonic Rotor Rig Cross Section at the Naval Postgraduate
School. Source: [7].

The resulting heat flux and overall heat transfer coefficients (*h*) are presented in Figures 3 and 4, respectively.
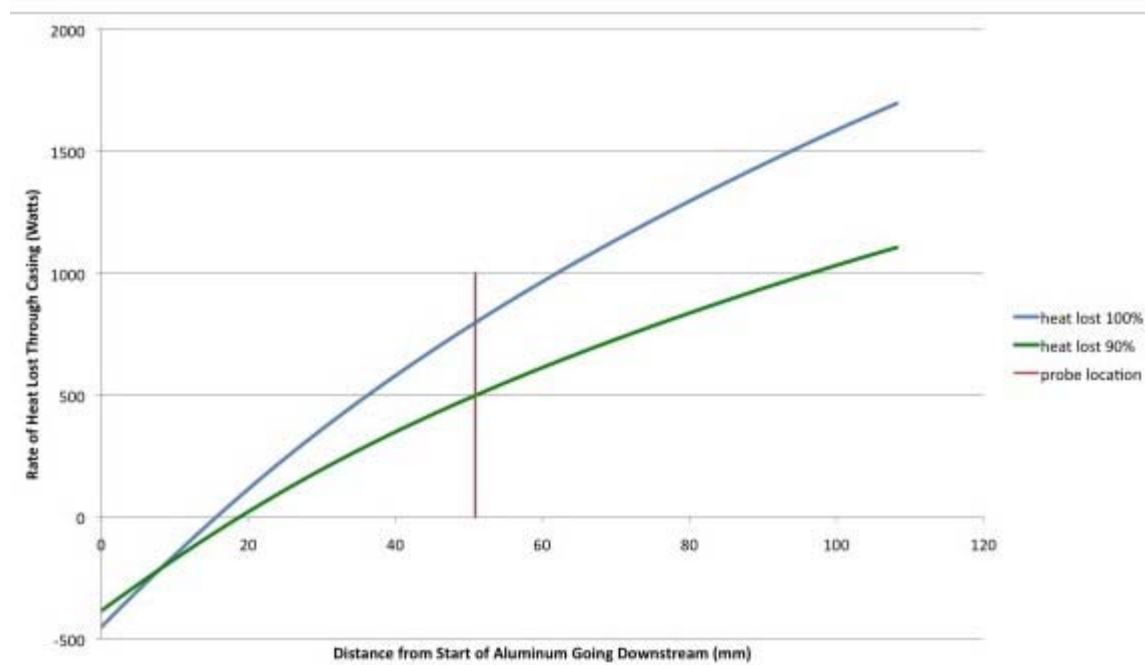


Figure 3.     Net Cumulative Heat Lost through the Casing for 100% and 90%
Speed. Source: [7].
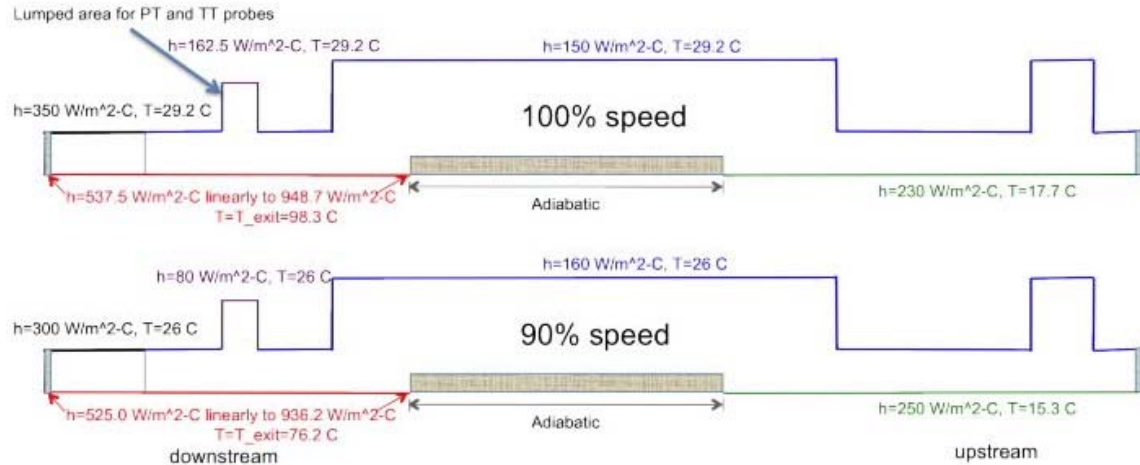
Figure 4.    Boundary Conditions for the Heat Transfer Analysis. Source: [7].

Both ends and the region right above the rotor are considered adiabatic therefore heat loss occurs only upstream of the total pressure (PT) and total temperature (TT) probes and downstream of the rotor. Heat transfer coefficients are twice as high downstream of the rotor and are relatively high. Additionally, the tests resulted in efficiencies 0.36% and 0.29% higher than the adiabatic efficiencies for 100% and 90% speeds, respectively. A stator would generally sit in the region downstream of the rotor and could increase heat transfer even more.

## 4.    Heat Pipes

Heat pipes are devices used to transfer thermal energy from one solid interface to another by means of convection and conduction; most commonly used for cooling [9]. A heat pipe is comprised of three basic components, a working fluid, a wick or capillary structure and a containing body (tube) [10]. The walls of the sealed hollow tube are lined with the capillary structure and the thermodynamic working fluid saturates the pores of the wick [11]. The working fluid must be in thermodynamic equilibrium, where saturated liquid and vapor coexist, in order for heat transfer to occur. The working fluid absorbs thermal energy from the heat source (high temperature area), evaporating into vapor. The vapor then travels along the pipe, carrying the thermal energy to the heat sink (low temperature end). At the heat sink, the vapor condenses into liquid, releasing the thermal energy. The wick absorbs the working fluid, which then flows back to the heat source

5

where the process repeats continuously [12]. This thermal cycle of a heat pipe is illustrated in Figure 5.
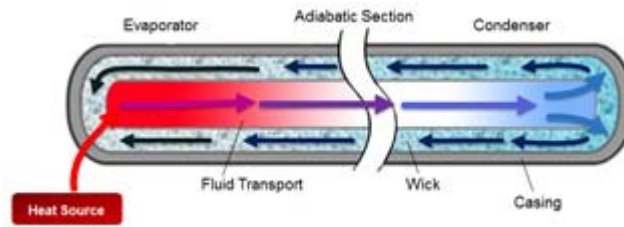


Figure 5.    Heat Pipe Thermal Cycle. Source: [13].

As indicated above thermal energy is only transferred between interfaces at the heat source and heat sink. No heat transfer occurs along the pipe, the region between the heat source and heat sink; this section is adiabatic. A suitable working fluid is chosen based on the desired operating vapor temperature range for a particular application. Table 1 lists the most common working fluids and their respective operating ranges.

Table 1.    Heat Pipe Working Fluids. Adapted from [10].

| Fluid | Melting Point (°C) | Boiling Point (°C) | Useful Range (°C) |
|---|---|---|---|
| Helium | -271 | -261 | (-271) - (-269) |
| Nitrogen | -210 | -196 | (-203) - (-160) |
| Ammonia | -78 | -33 | (-60) - (-100) |
| Pentane | -130 | 28 | (-20) - (120) |
| Acetone | -95 | 57 | 0 - 120 |
| Methanol | -98 | 64 | 10 - 130 |
| Ethanol | -112 | 78 | 0 - 130 |
| Heptane | -90 | 98 | 0 - 150 |
| Water | 0 | 100 | 30 - 200 |
| Toluene | -95 | 110 | 50 - 200 |
| Mercury | -39 | 361 | 250 - 650 |
| Caesium | 29 | 670 | 450 - 900 |
| Potassium | 62 | 774 | 500 - 1000 |
| Sodium | 98 | 892 | 600 - 1200 |
| Lithium | 179 | 1340 | 1000 - 1800 |
| Silver | 960 | 2212 | 1800 - 2300 |

Heat pipes have multiple applications. The simplest application is the extensive use of heat pipes in computer systems to cool the central processing units (CPUs). Via the thermal cycle described above, the heat pipe removes thermal energy (heat) from the CPU and transfers it to heat a sink where it can be dissipated into the environment [14]. A more advanced application is the use of heat pipes in internal combustion engines.

Internal combustion engines have combustion chambers with temperatures as high as 2700 K. Other component materials within the engine cannot withstand these high temperatures and thus some form of heat transfer must occur. Some internal combustion engines conduct heat transfer in the exhaust system. The exhaust valves have hollow stems containing sodium, which act as heat pipes with sodium being the working fluid. These hollow stems remove heat from the face area of the valve, preventing damage [15].

## C.    OVERVIEW

This thesis is a study into the feasibility of embedding heat exchange systems within engines.  It begins with an evaluation of the performance of the basic Brayton cycle with a maximum cycle temperature of 1700 K.  The performance gains of typical cycle modifications are also analyzed and compared.  Next, using thermodynamic and heat transfer theory, a means to compute an effectiveness of an integrated heat exchange system, which transfers heat from existing blade surfaces, is derived via the NTU method.  Experimental heat transfer data obtained from a transonic rotor rig is then used to compute the effectiveness of this system.  Finally, the resulting effectiveness is used to determine the performance gains associated with integrated heat exchange and compared to the performance of the basic Brayton cycle.  While this is an investigation into the incorporation of embedded heat exchangers using existing stator blade geometry, engines could be modified to improve the heat transfer of a particular stator stage.  The actual performance gain would then lie between what is presented here and a fully recuperated engine.

THIS PAGE INTENTIONALLY LEFT BLANK

## II.     ANALYSIS OF BRAYTON CYCLES

Many jet propulsion engines are simply an internal combustion, open-cycle gas turbine. The air-standard Brayton cycle is the typical cycle for the simple gas turbine [16]. The components of a Brayton cycle gas turbine for jet propulsion are shown in Figure 6.
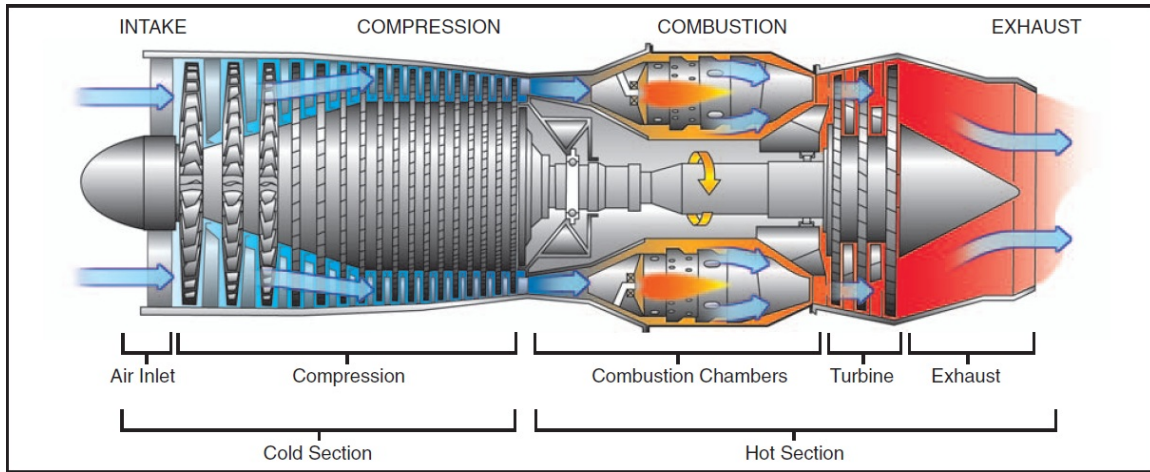


Figure 6.     Basic Components of a Gas Turbine Engine. Source: [17].

Air from the surrounding atmosphere enters the air inlet. After compression, air enters the combustion chamber where fuel is injected for combustion. The products resulting from combustion drive the turbine as they expand. The combustion products are then exhausted to the atmosphere.

There are multiple Brayton cycle modifications that can be made to improve cycle efficiency and/or specific power.

### A.     THERMODYNAMIC THEORY

#### 1.     First Law of Thermodynamics

The first law of thermodynamics states that energy can neither be created nor destroyed, but transformed from one form to another [13]; from heat into work and vice

versa. Thus, for a steady-state process the total energy entering the control volume must be equal to the total energy exiting the control volume. The first law of thermodynamics for a steady-state control volume is

$$q + h_i + \frac{v_i^2}{2} + gZ_i = h_e + \frac{v_e^2}{2} + gZ_e + w. \tag{1}$$

For a jet engine, it is assumed that there is no change in height (Z) and the velocity of the air is relatively constant across the control volume simplifying Equation (1) to

$$q + h_i = h_e + w \tag{2}$$

$$q - w = h_e - h_i = \Delta h. \tag{3}$$

For an ideal gas,

$$\Delta h = C_p \Delta T. \tag{4}$$

Thus, Equation (3) becomes

$$q - w = C_p \Delta T. \tag{5}$$

In this analysis, each individual component of the Brayton cycle is a steady-state control volume.

### a. *Compressor*

A compressor is assumed adiabatic (q=0) and requires an input of work energy.

$$w = -C_p \Delta T \tag{6}$$

### b. *Combustion Chamber*

A combustion chamber is a constant pressure heat exchanger requiring a heat input but no work (w=0).

$$q = C_p \Delta T \tag{7}$$

### c. *Turbine*

Like a compressor, the turbine is also considered adiabatic but instead yields work output.

$$w = C_p \Delta T \tag{8}$$

## 2. Thermal Efficiency

The thermal efficiency (η) of the Brayton cycle is defined as the ratio of the network to the heat input.

$$\eta = \frac{w_{net}}{Q_{in}} = \frac{w_{out} - w_{in}}{Q_{in}} \tag{9}$$

## 3. Specific Power

The specific power is equal to the net cycle work ($w_{net}$).

$$w_{net} = w_{out} - w_{in} \tag{10}$$

## B. BASIC BRAYTON CYCLE

The basic Brayton cycle utilizes two constant-pressure and two isentropic processes [13]. As seen in the temperature-entropy (T-S) diagram in Figure 7, compression and expansion in the compressor and turbine, respectively, is isentropic and the combustion chamber operates at constant pressure.
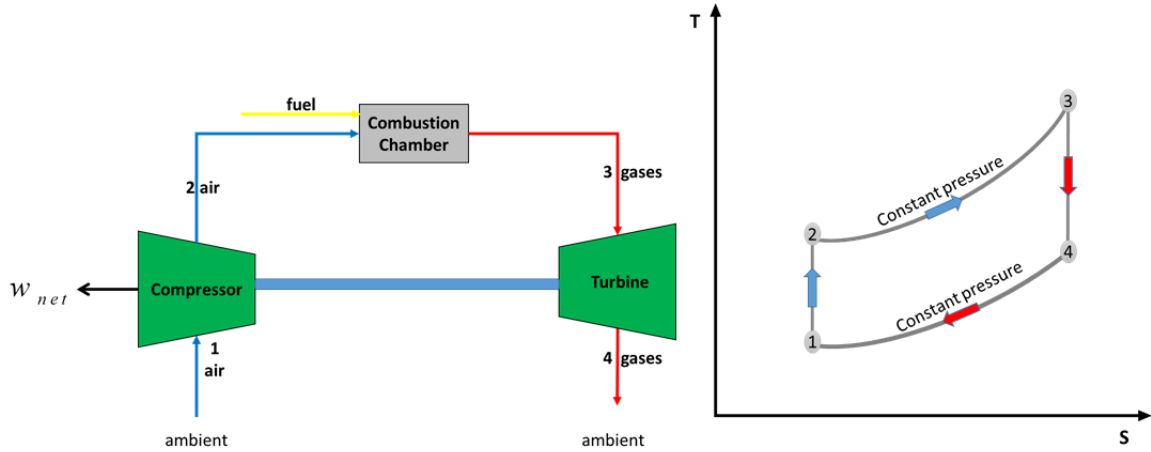


Figure 7.    Schematic of Basic Brayton Cycle

From Equations (6) through (8), the cycle efficiency can be determined.

$$w_{out} = w_{turb} = C_p \Delta T = C_p (T_4 - T_3) \tag{11}$$

$$w_{in} = w_{comp} = C_p \Delta T = C_p (T_2 - T_1) \tag{12}$$

$$Q_{in} = q_{comb} = C_p \Delta T = C_p (T_3 - T_2) \tag{13}$$

Substituting into Equation (9),

$$\eta = \frac{C_p (T_4 - T_3) - C_p (T_2 - T_1)}{C_p (T_3 - T_2)} = \frac{(T_4 - T_3) - (T_2 - T_1)}{(T_3 - T_2)} . \tag{14}$$

The specific power is simply the net cycle work.

$$w_{net} = w_{out} - w_{in} = w_{turb} - w_{comp} = C_p (T_4 - T_3) - C_p (T_2 - T_1) \tag{15}$$

A compressor inlet temperature ($T_1$) of 288.15 K and a conservative turbine inlet temperature ($T_3$) of 1700 K are assumed [18] based on the take-off conditions of a gas turbine circa 2000. These will be used as the reference points for all calculations in this study. The constant-pressure specific heat capacity ($C_p$) of air is also known.

The assumption of isentropic compression and expansion is used to determine the compressor outlet temperature ($T_2$) and the turbine outlet temperature ($T_4$) as a function of compressor pressure ratio $\left( \dfrac{P_2}{P_1} \right)$. For isentropic compression of an ideal gas,

$$\frac{P_2}{P_1} = \left( \frac{T_2}{T_1} \right)^{\frac{\gamma}{\gamma - 1}}, \tag{16}$$

where $\gamma$ is the specific heat ratio of air. Rearranging to solve for the compressor outlet temperature,

$$T_2 = T_1 \left( \frac{P_2}{P_1} \right)^{\frac{\gamma - 1}{\gamma}} . \tag{17}$$

As shown on the T-S diagram in Figure 7, due to the constant-pressure operation of the combustion chamber, the compressor outlet pressure ($P_2$) is equal to the turbine inlet

pressure ($P_3$). Also, the turbine exhausts back into the atmosphere; therefore, $P_4 = P_1$, thus applying the isentropic assumption to the turbine yields

$$\frac{P_4}{P_3} = \left(\frac{T_4}{T_3}\right)^{\frac{\gamma}{\gamma-1}} = \frac{P_1}{P_2} . \tag{18}$$

Rearranging to solve for turbine outlet temperature,

$$T_4 = T_3 \left(\frac{P_1}{P_2}\right)^{\frac{\gamma-1}{\gamma}} . \tag{19}$$

From Equations (17) and (19), along with the reference points defined above, the temperatures at all stages of the cycle are known. These, along with the known constants, are used to determine the cycle efficiency and specific power from Equations (14) and (15), respectively.

## C.    BRAYTON CYCLE WITH REHEAT

The reheat Brayton cycle allows for two heat additions. This requires two turbines and two combustion chambers. The plant efficiency decreases slightly but the specific work increases considerably resulting in a more compact machine.    Figure 8 is a schematic of the reheat Brayton cycle and its T-S diagram.
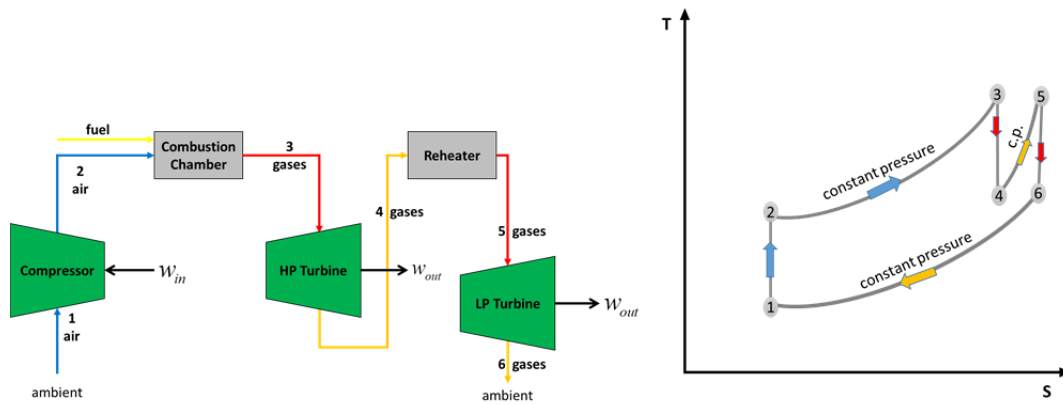


Figure 8.    Schematic of Reheat Brayton Cycle

In order to determine the specific work and cycle efficiency, Equations (6) through (8) are applied to each cycle component appropriately to find the work or heat energy associated with each process.

$$w_{in} = w_{comp} = C_p \Delta T = C_p (T_2 - T_1) \tag{20}$$

In this cycle, there are two turbines thus two sources of work output.

$$w_{out} = w_{turb} = (C_p \Delta T)_{HP} + (C_p \Delta T)_{LP} = C_p (T_4 - T_3) + C_p (T_6 - T_5) \tag{21}$$

There are also two combustion chambers thus two sources of heat input.

$$q_{in} = (C_p \Delta T)_{comb} + (C_p \Delta T)_{reheat} = C_p (T_3 - T_2) + C_p (T_5 - T_4) \tag{22}$$

The specific power ( $w_{net}$ ) and cycle efficiency are then,

$$w_{net} = C_p (T_4 - T_3) + C_p (T_6 - T_5) - C_p (T_2 - T_1) = C_p [(T_4 - T_3) + (T_6 - T_5) - (T_2 - T_1)] \tag{23}$$

$$\eta = \frac{w_{net}}{q_{in}} = \frac{(T_4 - T_3) + (T_6 - T_5) - (T_2 - T_1)}{(T_3 - T_2) + (T_5 - T_4)}. \tag{24}$$

The compressor inlet temperature ( $T_1$ ) and the turbine inlet temperatures ( $T_3$ and $T_5$ ) of 288.15 K and 1700 K, respectively, will continue to be used as reference points. Thus, the compressor outlet temperature ( $T_2$ ) can be computed as a function of compressor pressure ratio $\left( \dfrac{P_1}{P_2} \right)$ using the isentropic relationship in Equation (16). Assuming isentropic expansion of an ideal gas,

$$\frac{T_3}{T_4} = \left( \frac{P_3}{P_4} \right)^{\frac{\gamma - 1}{\gamma}} \tag{25}$$

$$\frac{T_5}{T_6} = \left( \frac{P_5}{P_6} \right)^{\frac{\gamma - 1}{\gamma}}, \tag{26}$$

and further assuming the pressure ratios of both turbines are equal,

$$\frac{P_3}{P_4} = \frac{P_5}{P_6}, \tag{27}$$

results in the following turbine outlet temperature ratio:

14

$$\frac{T_3}{T_4} = \frac{T_5}{T_6}.$$ (28)

Since the turbine inlet temperatures are fixed and equal the turbine outlet temperatures will also be equal.

$$T_4 = T_6$$ (29)

With all the pressure ratios known the turbine outlet temperature ($T_4$) can be computed as a function of compressor pressure ratio $\left(\frac{P_2}{P_1}\right)$ and turbine inlet temperature ($T_3$). As seen in the T-S diagram in Figure 8,

$$\frac{P_2}{P_1} = \frac{P_3}{P_6},$$

and

$$\frac{P_3}{P_6} = \frac{P_3}{P_4}\frac{P_5}{P_6} = \frac{P_3}{P_4}\frac{P_3}{P_4},$$

meaning

$$\frac{P_2}{P_1} = \left(\frac{P_3}{P_4}\right)^2,$$

then

$$\frac{P_3}{P_4} = \sqrt{\frac{P_2}{P_1}}.$$ (30)

Substituting Equation (30) into Equation (25) yields,

$$\frac{T_3}{T_4} = \left(\sqrt{\frac{P_2}{P_1}}\right)^{\frac{\gamma-1}{\gamma}}.$$ (31)

And finally, rearranging Equation (31) to solve for turbine outlet temperature ($T_4$) yields,

$$T_4 = T_3\left(\sqrt{\frac{P_2}{P_1}}\right)^{\frac{\gamma-1}{\gamma}}.$$ (32)

From Equations (17) and (32), along with the reference points, the temperatures at all stages of the cycle are known. These, along with the known constants, are used to

15

determine the specific power and cycle efficiency from Equations (23) and (24), respectively.

## D. BRAYTON CYCLE WITH REGENERATION

Since the temperature of the exhaust gases from the turbine is higher than the compressor outlet temperature of a gas turbine engine, a counter-flow heat exchanger can be used to transfer heat from the exhaust gases to the air leaving the compressor [19]. This increases the temperature of the air prior to entering the combustion chamber, decreasing the necessary heat input and fuel required for the same work output, which ultimately results in a higher cycle efficiency. A counter-flow heat exchanger used in this application is called a regenerator. A schematic of a regenerative Brayton cycle and its associated T-S diagram are shown in Figure 9.
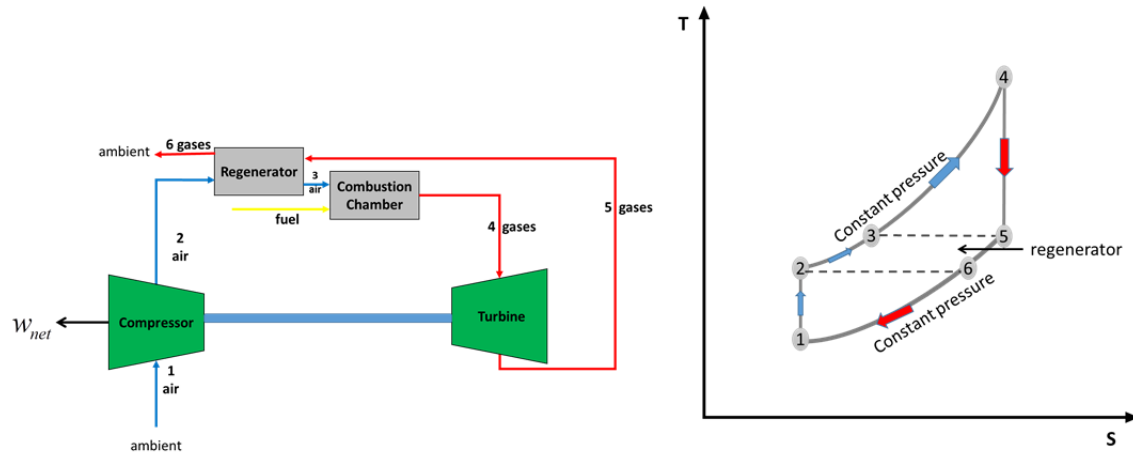


Figure 9.    Schematic of Regenerative Brayton Cycle

The specific power and efficiency of the regenerative cycle can be computed in the same fashion as the basic cycle. As before, compressor inlet temperature $(T_1)$ and the turbine inlet temperature $(T_4)$ are assumed fixed and used as reference points. The compressor work is again determined by assuming isentropic compression of an ideal gas using Equation (17) to find the compressor outlet temperature as a function of

16

compressor pressure ratio $\left(\dfrac{P_2}{P_1}\right)$ and Equation (12) to compute the work required. In order to find the cycle work produced Equation (8) must be applied to the turbine.

$$w_{out} = w_{turb} = C_p \Delta T = C_p (T_4 - T_5) \tag{33}$$

Next, Equation (7) is applied to the combustion chamber in order to determine the amount of heat input required.

$$q_{in} = C_p \Delta T = C_p (T_5 - T_4) \tag{34}$$

Equations (32) through (34) are then plugged into Equations (9) and (10) to solve for the cycle efficiency and specific power.

$$w_{net} = w_{out} - w_{in} = C_p (T_5 - T_4) - C_p (T_2 - T_1) = C_p [(T_5 - T_4) - (T_2 - T_1)] \tag{35}$$

$$\eta = \frac{w_{net}}{q_{in}} = \frac{w_{out} - w_{in}}{q_{in}} = \frac{(T_5 - T_4) - (T_2 - T_1)}{(T_4 - T_3)} \tag{36}$$

As stated previously, compressor inlet temperature $(T_1)$ and turbine inlet temperature $(T_4)$ are assumed fixed reference points. Compressor outlet temperature

$(T_2)$ is found, assuming isentropic compression of an ideal gas, using Equation (16). Assuming ideal operation of the regenerator or perfect heat exchanger effectiveness, the combustion chamber inlet temperature $(T_3)$ is equal to the turbine outlet temperature $(T_5)$. The turbine outlet temperature can be found by applying the isentropic expansion of an ideal gas assumption.

$$\frac{T_4}{T_5} = \left(\frac{P_4}{P_5}\right)^{\frac{\gamma-1}{\gamma}} \tag{37}$$

Rearranging to solve for $T_5$ and assuming the turbine pressure ratio $\left(\dfrac{P_4}{P_5}\right)$ is equal to the

compressor pressure ratio $\left(\dfrac{P_2}{P_1}\right)$, as seen in the T-S diagram of Figure (8), Equation (37) becomes

$$T_5 = \frac{T_4}{\left(\dfrac{P_2}{P_1}\right)^{\frac{\gamma-1}{\gamma}}}. \tag{38}$$

## E.    BRAYTON CYCLE WITH INTERCOOLING

A Brayton cycle with intercooling uses two or more compression stages and intercoolers to reduce the power required for compression, increasing the specific power obtained from the cycle. This also, however, increases the heat requirement resulting in a slight decrease in cycle efficiency at higher pressure ratios [16]. In this analysis, a cycle with two compressors of equal pressure ratio and one intercooler, as shown in Figure 10, is studied. Following the first compression stage, an intercooler returns the air to the cycle inlet temperature before it is compressed in a second stage. This is seen in the T-S diagram of Figure 10.
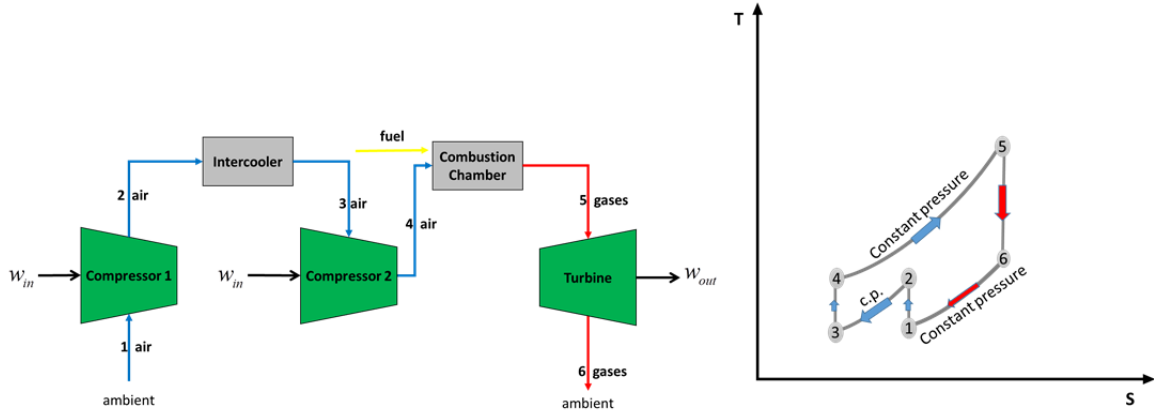


Figure 10.    Schematic of Brayton Cycle with Intercooling

To determine the cycle efficiency and specific power, the work and/or heat of each cycle component must again be computed. A few assumptions must be first be made. For this analysis, it is assumed that both compressors have the same pressure ratio $\left(\dfrac{P_2}{P_1} = \dfrac{P_4}{P_3}\right)$. It is also assumed that the intercooler cools the air to first compressor inlet temperature $(T_1 = T_3)$.

Beginning with Equation (12) and taking into account that the cycle utilizes two compressors, the work required is found with Equation (39)

$$w_{in} = w_{comp1} + w_{comp2} = C_p(T_2 - T_1) + C_p(T_4 - T_3) = C_p[(T_2 - T_1) + (T_4 - T_3)]. \tag{39}$$

Next, the cycle work output is found and Equation (8) becomes

$$w_{out} = w_{turb} = C_p(T_5 - T_6). \tag{40}$$

Lastly, cycle heat input is found and Equation (7) becomes

$$q_{in} = C_p(T_5 - T_4). \tag{41}$$

Equations (39) through (41) can now be plugged into Equations (9) and (10) to solve for the specific power and cycle efficiency.

$$w_{net} = w_{out} - w_{in} = C_p[(T_5 - T_6) - ((T_2 - T_1) + (T_4 - T_3))] \tag{42}$$

$$\eta = \frac{w_{net}}{q_{in}} = \frac{(T_5 - T_6) - [(T_2 - T_1) + (T_4 - T_3)]}{(T_5 - T_4)} \tag{43}$$

Both compressor inlet temperatures ($T_1$ and $T_3$), as well as the turbine inlet temperature ($T_5$), are known reference points. The compressor outlet temperatures ($T_2$ and $T_4$) can be calculated using Equations (17) and (19), respectively. The turbine outlet temperature ($T_6$) can be computed as a function of compressor pressure ratio $\left(\dfrac{P_2}{P_1}\right)$ by applying the isentropic expansion of an ideal gas assumption,

$$\frac{T_5}{T_6} = \left(\frac{P_5}{P_6}\right)^{\frac{\gamma-1}{\gamma}}, \tag{44}$$

and, as indicated in the T-S diagram of Figure 10,

$$\frac{P_5}{P_6} = \frac{P_4}{P_1} = \frac{P_4}{P_3}\frac{P_2}{P_1}.$$

Recalling the assumption of equal compressor pressure ratios,

$$\frac{P_5}{P_6} = \left(\frac{P_2}{P_1}\right)^2.$$

Substituting the above ratio into Equation (44) then yields

$$\frac{T_5}{T_6} = \left[ \left( \frac{P_2}{P_1} \right)^2 \right]^{\frac{\gamma-1}{\gamma}}. \tag{45}$$

Rearranging to solve for $T_6$, Equation (45) becomes

$$T_6 = \frac{T_5}{\left[ \left( \frac{P_2}{P_1} \right)^2 \right]^{\frac{\gamma-1}{\gamma}}}. \tag{46}$$

## F.  BRAYTON CYCLE WITH ISOTHERMAL COMPRESSION

A Brayton cycle with isothermal compression utilizes all the same components as the basic cycle, only the compressor is assumed to operate isothermally, meaning the compressor outlet temperature is equal to its inlet temperature $(T_2 = T_1)$. This is illustrated by the constant temperature line between the first two points of the T-S diagram in Figure 11.
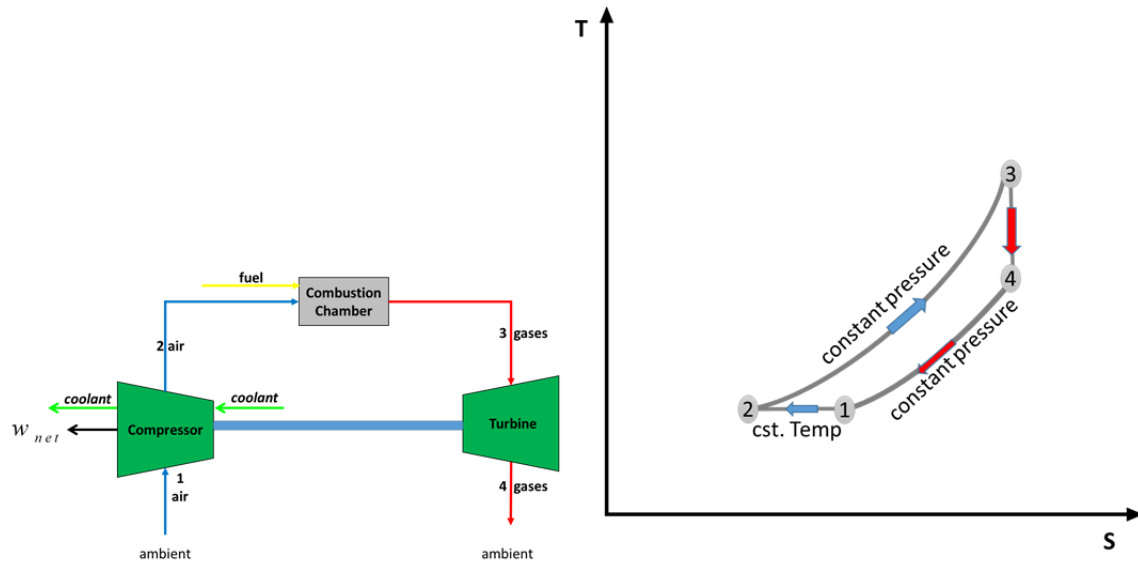


Figure 11.   Schematic of Brayton Cycle with Isothermal Compression

20

The specific power and efficiency of this cycle is determined by applying the isothermal condition to Equations (14) and (15).

$$w_{net} = C_p[(T_4 - T_3) - (T_2 - T_1)] = C_p[(T_4 - T_3) - 0] = C_p(T_4 - T_3) \qquad (47)$$

$$\eta = \frac{(T_4 - T_3) - (T_2 - T_1)}{(T_3 - T_2)} = \frac{(T_4 - T_3) - 0}{(T_3 - T_2)} = \frac{(T_4 - T_3)}{(T_3 - T_2)} \qquad (48)$$

The compressor outlet temperature $(T_2)$ is equal to the compressor inlet temperature $(T_1)$ which, along with the turbine inlet temperature $(T_3)$, is a known reference point. The turbine outlet temperature $(T_4)$ can be calculated using Equation (19).

## G.    CYCLE COMPARISON

Using the Equations derived from the thermodynamic theory in this chapter, the efficiency and specific power of each modified cycle were calculated for a range of compressor pressure ratios and compared to the efficiency and normalized specific power of the ideal basic Brayton cycle. The results of these calculations are presented in Figures 12 and 13. As mentioned previously, the specific power output of the regenerative Brayton cycle is equal to that of the basic Brayton cycle, so these lines are plotted on top of one another in Figure 13.
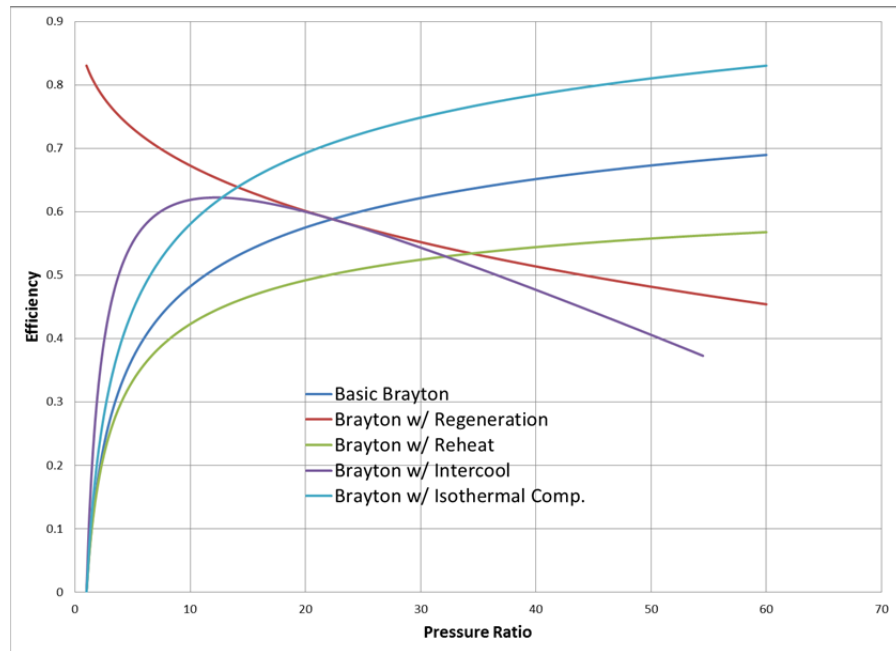
Figure 12.    Cycle Efficiency versus Compressor Pressure Ratio
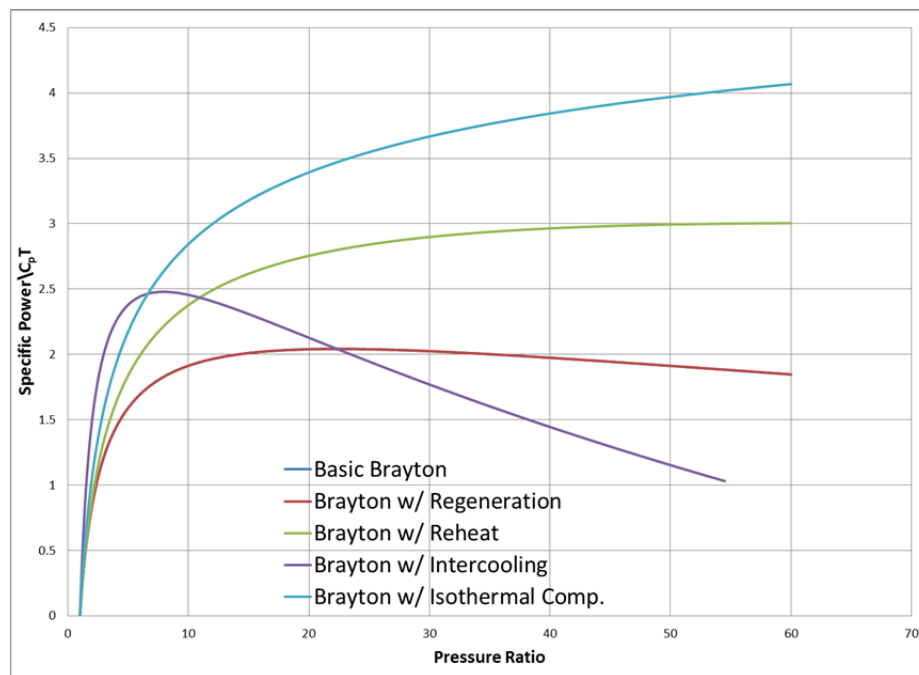


Figure 13.    Specific Power versus Compressor Pressure Ratio

The reheat Brayton cycle produces more specific power than the basic cycle but is consistently less efficient than the basic cycle. The efficiency of the regenerative cycle, however, is greater than that of basic cycle for pressure ratios less than 20, for the same work output, while the basic cycle is more efficient at pressure ratios greater than 20. The Brayton cycle with intercooling is more efficient and yields a greater amount of power for pressure ratios of 25 or less, while the basic cycle is more efficient and produces more work for ratios greater than 25. Lastly, isothermal compression makes the cycle consistently more efficient and yields more work output than the basic cycle across the board.

While these cycle modifications appear to be quite favorable, whether the goal is to increase efficiency or work output, it is only feasible to apply this technology to land based gas turbines. Transferring this technology to aviation and ship gas turbines is difficult due to the size and weight of the additional components required. An alternate approach would be to embed a heat exchange system within the engine using existing blade surfaces to extract and insert heat.

THIS PAGE INTENTIONALLY LEFT BLANK

# III. PERFORMANCE GAIN WITH INTEGRATED HEAT EXCHANGE

Due to the highly turbulent and transient flow, heat transfer coefficients in turbomachinery are extremely high, making it possible to embed a heat exchange system within the engine. Heat transfer between the turbine and compressor blade surfaces would be accomplished using compact exchange devices such as evaporative heat pipes. Thermal energy would be transferred from the hot section of the engine to the cold section as in Figure 14.
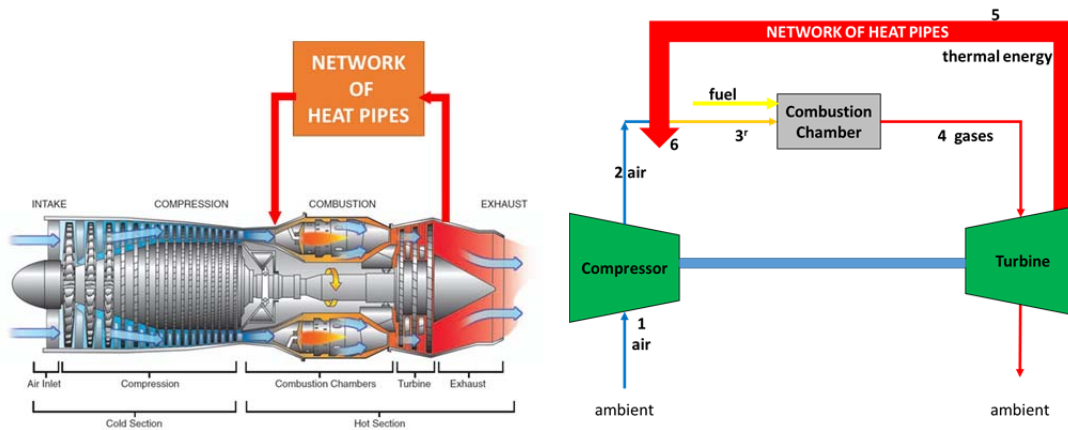


Figure 14.    Schematic of Engine with Integrated Heat Exchange.
Adapted from [17]

The addition of heat pipes would add very little weight with to existing engines and be completely passive, requiring no additional control systems. These advantages make this a more feasible approach to increase efficiency in aviation engines than the cycle modifications discussed in the previous chapter.

## A.    EQUIVALENT HEAT EXCHANGER EFFECTIVENESS

### 1.    Heat Transfer Theory

The effectiveness ($\varepsilon$) of a heat exchanger is the ratio of the actual heat transfer rate to the maximum possible heat transfer rate [20]:

$$\varepsilon = \frac{q}{q_{max}}. \tag{49}$$

The number of transfer units ( $NTU$ ) is a dimensionless parameter that is widely used for heat exchanger analysis and is defined as [20]

$$NTU = \frac{UA}{C_{min}}, \tag{50}$$

where $U$ is the overall heat transfer coefficient, $A$ is total area of heat exchange surfaces and $C = \dot{m}C_p$. For any heat exchanger, effectiveness is a function of NTU and specific heat capacity,

$$\varepsilon = f(NTU, C_r), \tag{51}$$

where $C_r = \frac{C_{min}}{C_{max}}$. For a counter-flow heat exchanger where both the hot and cold medium are the same fluid, in this case air, $C_r = 1$ and

$$\varepsilon = \frac{NTU}{NTU+1}. \tag{52}$$

In order to determine whether it is feasible to extract heat from the turbine blade surfaces and insert it onto the compressor blade surfaces, a means to calculate an equivalent heat exchanger effectiveness is derived using this NTU method.

Beginning with Equation (50),

$$NTU = \frac{UA}{C_{min}} = \frac{UA}{\dot{m}C_p}. \tag{53}$$

For a counter-flow heat exchanger, the surface area of the hot fluid section is equal to the surface area of the cold fluid section. This, however, is not always the case in a gas turbine engine, and a mean surface area ( $A_m$ ) must be defined as,

$$A_m = \frac{A_h + A_c}{2}. \tag{54}$$

Plugging Equation (54) into Equation (53) yields,

$$NTU = \frac{U(A_h + A_c)}{2\dot{m}C_p}, \tag{55}$$

where $A_h$ is the area of the hot section, surface of the turbine blades, and $A_c$ is the area of the cold section, surface of the compressor blades. Next, the overall heat transfer coefficient can be defined as,

$$\frac{1}{UA} = \frac{1}{UA_m} = \frac{1}{h_c A_c} + \frac{1}{h_h A_h}, \tag{56}$$

where $h_h$ and $h_c$ are the heat transfer coefficients of the engine hot and cold sections, respectively. Rearranging to solve for the overall heat transfer coefficient, Equation (56) becomes,

$$\frac{1}{U} = \frac{A_m}{(hA)_c} + \frac{A_m}{(hA)_h} = A_m \left( \frac{1}{(hA)_c} + \frac{1}{(hA)_h} \right) = A_m \left[ \frac{(hA)_c + (hA)_h}{(hA)_c (hA)_h} \right],$$

$$U = \frac{1}{A_m} \left[ \frac{(hA)_c (hA)_h}{(hA)_c + (hA)_h} \right], \tag{57}$$

and plugging (57) into (55) yields,

$$NTU = \frac{1}{A_m} \left[ \frac{(hA)_c (hA)_h}{(hA)_c + (hA)_h} \right] \frac{A_m}{\dot{m}C_p} = \frac{1}{\dot{m}C_p} \left[ \frac{(hA)_c (hA)_h}{(hA)_c + (hA)_h} \right]. \tag{58}$$

Equation (58) can be further simplified by defining an area ratio,

$$x = \frac{A_h}{A_c}, \tag{59}$$

solving for $A_c$ in terms of $A_h$,

$$A_c = xA_h, \tag{60}$$

and finally substituting Equation (60) into (58) yields

$$NTU = \frac{1}{\dot{m}C_p} \left[ \frac{(h_c xA_h)(hA)_h}{(h_c xA_h) + (hA)_h} \right] = \frac{A_h}{\dot{m}C_p} \left( \frac{x h_c h_h}{h_h + x h_c} \right) \tag{61}$$

## 2. Area of Integrated Heat Exchanger

In order to determine the effectiveness of an integrated heat exchange system using the NTU method derived above, it is necessary to find the total surface area of the turbine and compressor blades in which heat while be extracted and inserted. For the

purposes of this study, it is assumed that the area of the hot section ($A_h$) and area of the cold section ($A_c$) are equal.

Figure 15 is a diagram of a partial blade array and its dimensions, where $c$ is the chord, $s$ is the spacing between blades and $l$ is the blade height. The total blade area of stator comprised of $n$ two-sided blades is

$$A_b = 2ncl. \tag{62}$$
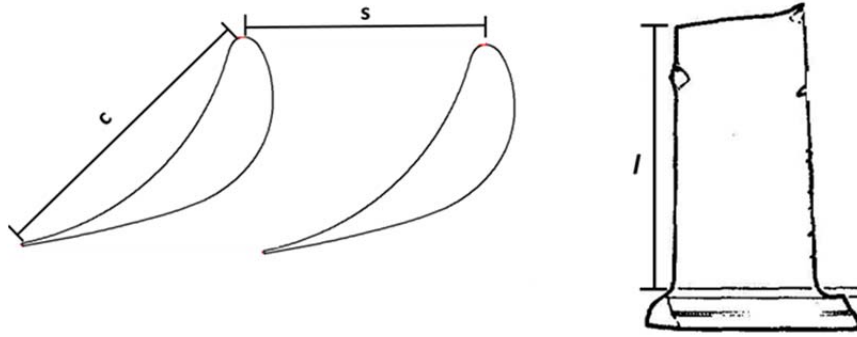


Figure 15.    Blade Dimensions. Adapted from [21]

A flow area ($A_f$) from which heat is transferred must be defined. In Figure 16 the stator is modeled as two concentric circles where the annulus is the flow area ($A_f$), $D_i$ is the diameter of the inner circle and $D_o$ is the diameter of the outer circle.
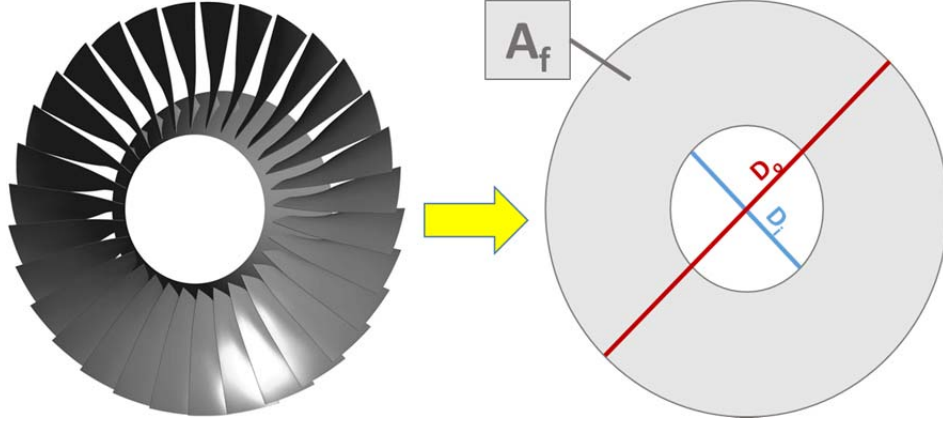
Figure 16.    Stator Dimensions

From the definition of mass flow rate

$$\dot{m} = \rho V_{ax} A_f ,$$

the flow area can be found as

$$A_f = \frac{\dot{m}}{\rho V_{ax}} , \tag{63}$$

where $\rho$ is the density of the flow and $V_{ax}$ is the axial velocity. This flow area is equal to the area of the annulus

$$A_f = \frac{\pi}{4}\left(D_o^2 - D_i^2\right). \tag{64}$$

Assuming a fixed diameter ratio,

$$\frac{D_i}{D_o} = 0.5 ,$$

solving for $D_i$ in terms of $D_o$,

$$D_i = 0.5 D_o ,$$

and substituting this into Equation (64) yields:

$$A_f = \frac{\pi}{4}\left[D_o^2 - (0.5 D_o)^2\right]. \tag{65}$$

Rearranging to solve for outer diameter, Equation (66) becomes

$$D_o = \sqrt{\frac{16A_f}{3\pi}},$$

(66)

and the inner diameter is then

$$D_i = 0.5\sqrt{\frac{16A_f}{3\pi}}.$$

(67)

The blade height is then the distance between the concentric circles,

$$l = \left(\frac{D_o}{2} - \frac{D_i}{2}\right),$$

(68)

and the chord is found using the definition of aspect ratio ($\phi$),

$$\phi = \frac{l}{c},$$

$$c = \frac{l}{\phi}.$$

(69)

From the blade solidity ($\sigma$) the spacing between blades is found.

$$\sigma = \frac{c}{s}$$

$$s = \frac{c}{\sigma}$$

(70)

The number of blades per stator is simply the ratio of stator circumference to blade spacing

$$n = \frac{\pi D_o}{s}.$$

(71)

Once the diameters and chord are known, the area of the casing ($A_{case}$) and the area of the hub ($A_{hub}$) can be calculated as follows.

$$A_{case} = \frac{\pi D_o c}{\sqrt{2}}$$

(72)

$$A_{hub} = \frac{\pi D_i c}{\sqrt{2}}$$

(73)

30

The total heat exchanger area is then

$$A_{tot} = A_h = A_c = A_b + A_{case} + A_{hub}. \tag{74}$$

It is also necessary to compute the hydraulic diameter ($D_h$),

$$D_h = 4\frac{A_p}{P}, \tag{75}$$

where $A_p$ is the passage flow area, defined as

$$A_p = \frac{A_f}{n}, \tag{76}$$

and $P$ is the passage perimeter, defined as

$$P = 2l + \frac{\pi D_o}{n} + \frac{\pi D_i}{n}. \tag{77}$$

## 3.    Data and Calculations

Gannon et al. [7] tested a highly loaded transonic fan with splittered rotor and a maximum pressure ratio of two. Conducting runs at 100% and 90% power, temperature and heat transfer data were obtained from two points of the casing. Using the observed heat transfer coefficient ($h$) and conductivity ($k$), as well as the measured hydraulic diameter ($D_h$) of the casing, an experimental Nusselt number ($Nu$) was calculated via Equation (78):

$$Nu = \frac{hD_h}{k}. \tag{78}$$

The experimental data and resulting Nusselt numbers are summarized in Table 3.

31

Table 2.     Experimental Data. Adapted from [7].

| | 100 % Run | | 90% Speed Run | |
|---|---|---|---|---|
| | Point 1 | Point 2 | Point 1 | Point 2 |
| Stagnant Temp. [K] | 369.820797 | 369.8207965 | 349.326649 | 349.3266491 |
| Stagnant Pressure | 124869.555 | 124869.5549 | 119944.623 | 119944.6231 |
| Static Pressure | 92910.9538 | 92910.95383 | 93615.6622 | 93615.66225 |
| Heat Xfer Coeff. [W/m²-K] | 948.7 | 537.5 | 936.2 | 525 |
| Conductivity (air) [W/m-K] | 0.03150638 | 0.031506381 | 0.02995017 | 0.029950172 |
| Outer Diameter [m] | 0.28702 | 0.28702 | 0.28702 | 0.28702 |
| Inner Diameter [m] | 0.233426 | 0.233426 | 0.233426 | 0.233426 |
| Hydraulic Diameter [m] | 0.053594 | 0.053594 | 0.053594 | 0.053594 |
| Nusselt No. | 1613.78828 | 914.3155929 | 1675.27261 | 939.4553716 |

Using the experimental Nusselt number and conductivity, as well as the theoretical hydraulic diameter computed via Equation (75), heat transfer coefficients for the hot and cold sections of an engine were computed using Equation (79)

$$h_h = h_c = \frac{Nu(k)}{D_h}.$$ (79)

From these heat transfer coefficients, the experimental data obtained and the conservative assumptions listed in Table 3, a theoretical heat exchanger effectiveness of the stator blades within a gas turbine engine is calculated via the NTU method derived in this chapter. Table 4 is a summary of the theoretical calculations and resulting effectiveness.

Table 3.     Assumptions

| Variable | Symbol | Assumed Value |
|---|---|---|
| Solidity | $\sigma$ | 1.2 |
| Aspect Ratio | $\phi$ | 1 |
| Diameter | $D_i/D_o$ | 0.5 |
| Mass flowrate | m | 1 kg/s |
| Axial Velocity | $V_{ax}$ | 100 m/s |

Table 4.    Effectiveness Calculations

| | | 100% Run | | 90% Run | |
|---|---|---|---|---|---|
| | | Point 1 | Point 2 | Point 1 | Point 2 |
| Mass Flow (kg/s) | $m$ | 1 | 1 | 1 | 1 |
| Axial Velocity (m/s) | $V_{ax}$ | 100 | 100 | 100 | 100 |
| Density (hot) (kg/m$^3$) | $\rho_h$ | 0.948554 | 0.948554 | 0.997507 | 0.997507 |
| Density (cold) (kg/m$^3$) | $\rho_c$ | 0.948554 | 0.948554 | 0.997507 | 0.997507 |
| Flow Area (m$^2$) | $A_f$ | 0.010542 | 0.010542 | 0.010025 | 0.010025 |
| Diameter (outer) (m) | $D_o$ | 0.133781 | 0.133781 | 0.130457 | 0.130457 |
| Diameter (inner) (m) | $D_i$ | 0.06689 | 0.06689 | 0.065228 | 0.065228 |
| Blade Height (m) | $l$ | 0.033445 | 0.033445 | 0.032614 | 0.032614 |
| Aspect Ratio | $\Phi$ | 1 | 1 | 1 | 1 |
| Chord (m) | $c$ | 0.033445 | 0.033445 | 0.032614 | 0.032614 |
| Solidity | $\sigma$ | 1.2 | 1.2 | 1.2 | 1.2 |
| Spacing (m) | $s$ | 0.027871 | 0.027871 | 0.027178 | 0.027178 |
| # of Blades | $n$ | 15.07964 | 15.07964 | 15.07964 | 15.07964 |
| Blade Area (m$^2$) | $A_B$ | 0.033736 | 0.033736 | 0.03208 | 0.03208 |
| Casing Area (m$^2$) | $A_{case}$ | 0.009939 | 0.009939 | 0.009452 | 0.009452 |
| Hub Area (m$^2$) | $A_{hub}$ | 0.00497 | 0.00497 | 0.004726 | 0.004726 |
| Total Area (m$^2$) | $A_{tot}$ | 0.048645 | 0.048645 | 0.046257 | 0.046257 |
| Specific Heat (J/Kg K) | $C_p$ | 1010.259 | 1010.259 | 1011.138 | 1011.138 |
| area ratio | $x$ | 1 | 1 | 1 | 1 |
| Nusselt No. | $Nu$ | 1613.788 | 369.8208 | 1675.273 | 939.4554 |
| Passage flow Area (m$^2$) | $A_p$ | 0.000699 | 0.000699 | 0.000665 | 0.000665 |
| Passage Perimeter (m) | $P$ | 0.108697 | 0.108697 | 0.105996 | 0.105996 |
| Hydraulic Diameter (m) | $D_h$ | 0.025727 | 0.025727 | 0.025088 | 0.025088 |
| conductivity (W/m-K) | $k$ | 0.031506 | 0.031506 | 3.00E-02 | 0.02995 |
| Heat xfer Coeff. (hot) (W/m$^2$ K) | $h_h$ | 1976.31 | 452.8974 | 1999.962 | 1121.534 |
| Heat xfer Coeff. (cold) (W/m$^2$ K) | $h_c$ | 1976.31 | 452.8974 | 1999.962 | 1121.534 |
| # of transfer units | NTU | 0.04758 | 0.010904 | 0.045747 | 0.025654 |
| Effectiveness | $\varepsilon$ | 0.04542 | 0.01079 | 0.04375 | 0.02501 |

33

## B. INTEGRATED REGENERATION

In Chapter II, the efficiency of a Brayton cycle with regeneration was computed assuming an ideal regenerator with 100% heat exchanger effectiveness. An equivalent heat exchanger effectiveness of an integrated recuperation system was found to be as high as 4.5%, as listed in Table 4. A real regeneration system with an effectiveness of 4.5% results in a lower combustion chamber inlet temperature, denoted $3^r$ in Figure 17, than ideal regeneration.
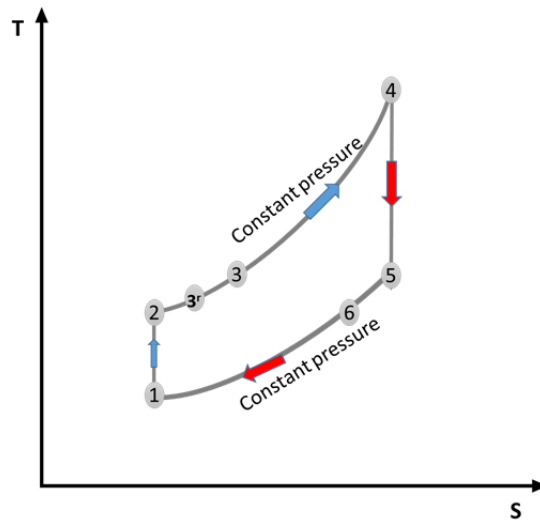


Figure 17.    T-S Diagram of Regenerative Cycle

The efficiency of the cycle with integrated regeneration can be calculated by substituting the combustion chamber inlet temperature for real regeneration ($T_{3^r}$) into Equation (36) which results in the following:

$$\eta = \frac{(T_4 - T_5) - (T_2 - T_1)}{(T_4 - T_{3^r})}.$$

(80)

The real combustion chamber inlet temperature ($T_{3^r}$) can be found using the integrated heat exchange effectiveness ($\varepsilon$) and the ideal temperatures.

$$\varepsilon = \frac{q}{q_{max}} = \frac{h_{3^r} - h_2}{h_3 - h_2} = \frac{C_p(T_{3^r} - T_2)}{C_p(T_3 - T_2)} = \frac{(T_{3^r} - T_2)}{(T_3 - T_2)}$$

(81)

34

Rearranging Equation (81) to solve for $T_{3r}$ yields:

$$T_{3r} = \varepsilon(T_3 - T_2) + T_2. \tag{82}$$

The ideal combustion chamber inlet temperature ($T_3$) and compressor outlet temperature ($T_2$) are found using Equations (38) and (16), respectively.

The efficiency of a Brayton cycle with integrated regeneration was computed for a range of compressor pressure ratios and compared to the basic Brayton cycle. The results are plotted in Figure 18.
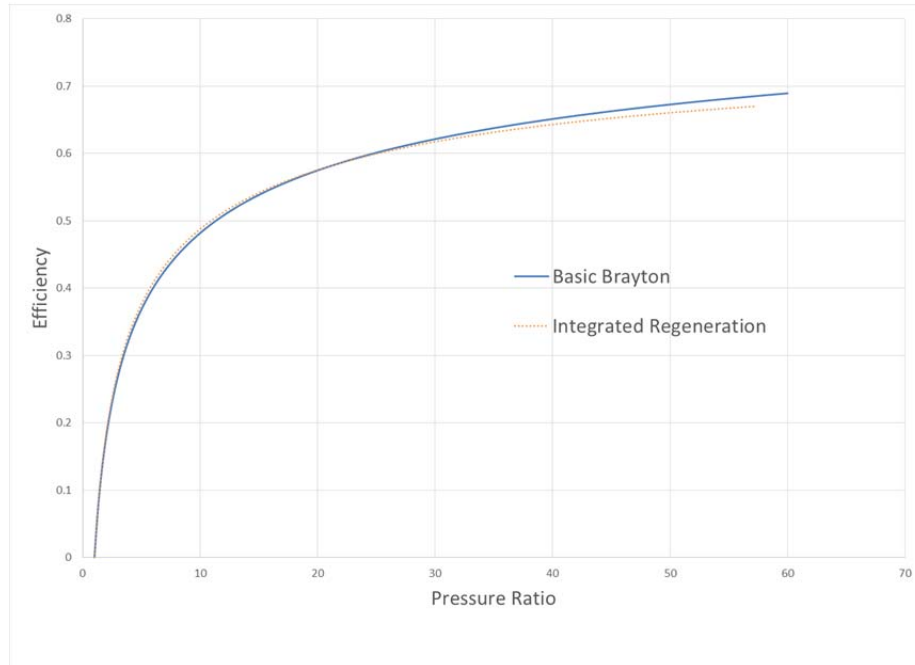


Figure 18.   Efficiency of Integrated Regeneration

## C.   INTEGRATED INTERCOOLING

An integrated heat exchange system can also be used to produce an intercooled cycle by removing heat and progressively cooling the flow as it is compressed.  This results in non-isentropic compression and a slightly lower compressor outlet temperature denoted by the dashed line between stages 1 and $2^r$ of the T-S diagram in Figure 19.
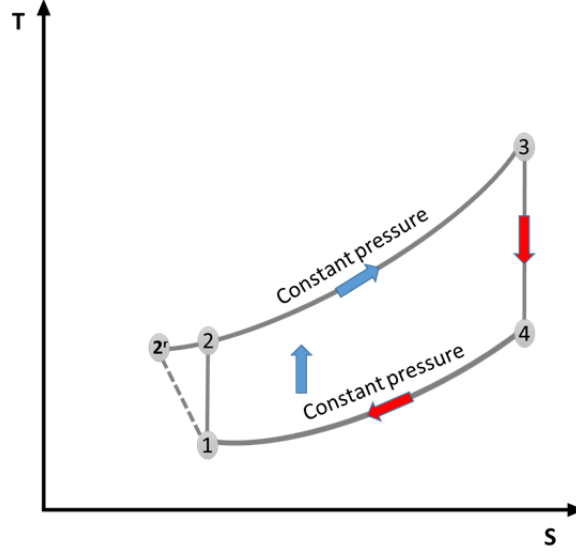
Figure 19.    T-S Diagram of Intercooled Cycle

The efficiency of the cycle with integrated intercooling can be calculated by substituting the non-isentropic compressor outlet temperature ($T_{2^r}$) into Equation (14) which results in the following:

$$\eta = \frac{(T_3 - T_4) - (T_{2^r} - T_1)}{(T_3 - T_{2^r})} . \tag{83}$$

The non-isentropic compressor outlet temperature ($T_{2^r}$) can be found using the integrated heat exchange effectiveness ($\varepsilon$) and the ideal, isentropic temperatures.

$$(1 - \varepsilon) = \frac{h_{2^r} - h_1}{h_2 - h_1} = \frac{C_p(T_{2^r} - T_1)}{C_p(T_2 - T_1)} = \frac{(T_{2^r} - T_1)}{(T_2 - T_1)} \tag{84}$$

Rearranging Equation (84) to solve for $T_{2^r}$ yields:

$$T_{2^r} = (1 - \varepsilon)(T_2 - T_1) + T_1 . \tag{85}$$

The compressor inlet temperature ($T_1$) is a known reference point and the isentropic compressor outlet temperature ($T_2$) is found using Equation (17).

The efficiency of a Brayton cycle with integrated intercooling was computed for a range of compressor pressure ratios and compared to the basic Brayton cycle. The results are plotted in Figure 20.
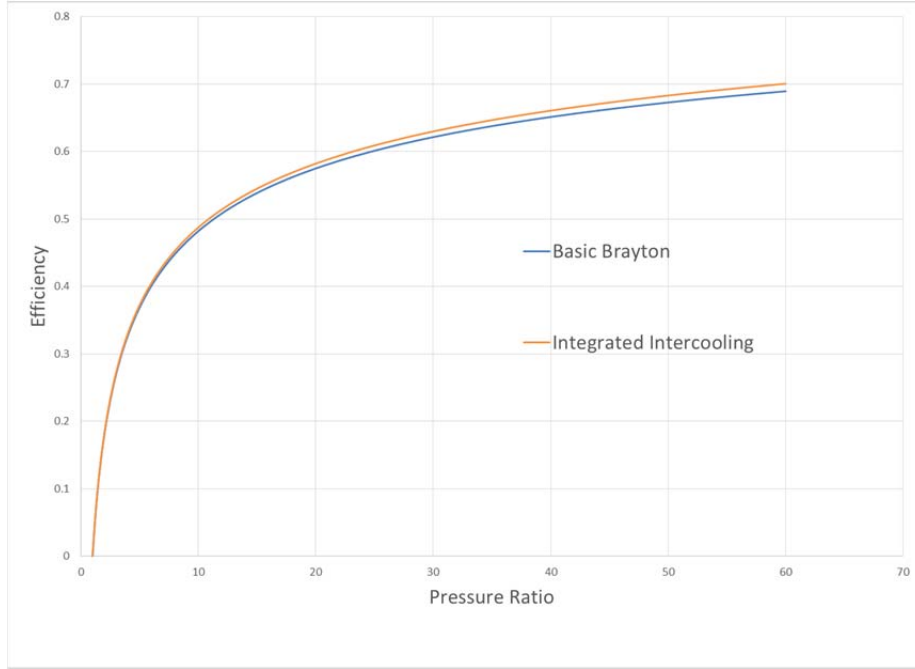
36

Figure 20.    Efficiency of Integrated Intercooling Cycle

The specific work of the cycle with integrated intercooling can be calculated by substituting the non-isentropic compressor outlet temperature ($T_{2^r}$) into Equation (15) which results in the following:

$$w_n = C_p(T_3 - T_4) - C_p(T_{2^r} - T_1) .(86)$$

The compressor and turbine inlet temperatures ($T_1$ and $T_3$) are known reference points. The turbine outlet temperature ($T_4$) and non-isentropic compressor outlet temperature ($T_{2^r}$) are found using Equations (19) and (85), respectively.

The specific power of a Brayton cycle with integrated intercooling was computed for a range of compressor pressure ratios and compared to the basic Brayton cycle. The results are plotted in Figure 21.
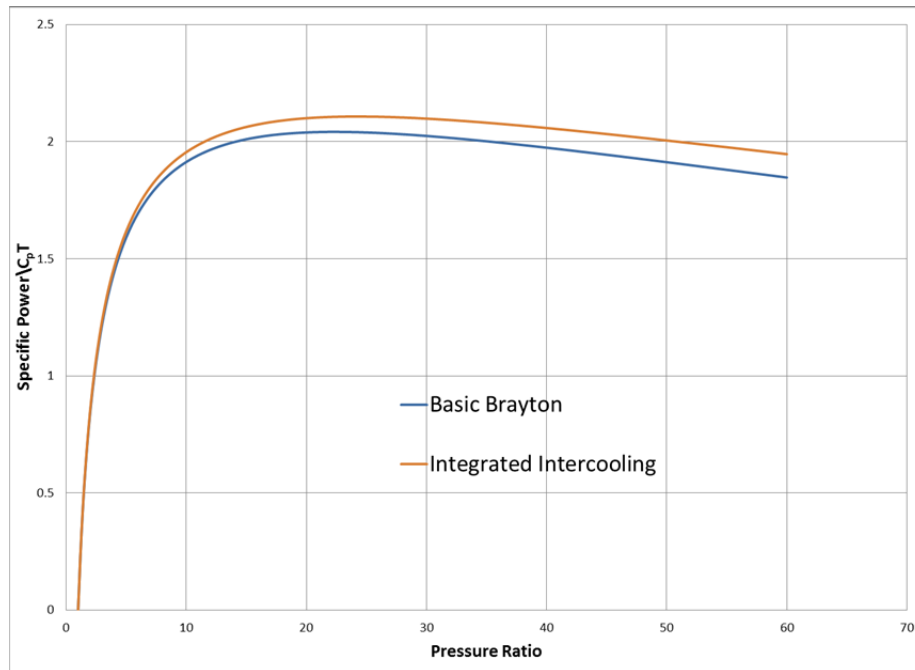
Figure 21.    Specific Power of Integrated Intercooling Cycle

# IV.  RESULTS AND CONCLUSIONS

## A.  SUMMARY OF RESULTS

### 1.  Common Ideal Cycle Modifications

Multiple Brayton Cycle modifications can be made to improve cycle efficiency and/or engine power output.  In this study, the efficiency and specific power output of a reheat cycle, regenerative cycle, intercooled cycle and a cycle with isothermal compression were computed, for a maximum cycle temperature of 1700 K, and compared to that of the basic Brayton cycle.

The reheat Brayton cycle produces 30-50% more power than the basic cycle.  This is due to the addition of a second turbine resulting in an increased work output.  This power increase, however, comes at the cost of efficiency.  In order to expand the gases across this second turbine, a reheater must also be used, increasing the amount of heat input required.  Thus, the reheat cycle is 5-10% less efficient than the basic cycle.

The regenerative Brayton cycle is more efficient than the basic cycle, at pressure ratios less than 22.  It is less efficient, compared to the basic cycle, at pressure ratios greater than 22.  Because there is no change in compressor or turbine work, the amount of power produced by the regenerative cycle is equal to that of the basic cycle.

Similar to the regenerative cycle, the intercooled Brayton cycle is more efficient at pressure ratios less than 22 and less efficient than the basic cycle at pressure ratios greater than 22.  The same is true for the amount power produced by the intercooled cycle compared to the basic cycle; more power at ratios less than 22 and less power for ratios greater than 22.

Lastly, applying isothermal compression to a basic Brayton cycle appears to greatly improve efficiency as well as power output, as there is virtually no compressor work required.  However, isothermal compression requires vast amounts of cooling.

## 2. Integrated Heat Exchange Effectiveness

Due to the highly turbulent and transient flow, heat transfer coefficients in turbomachinery are extremely high, making it possible to embed a heat exchange system within the engine. Heat transfer between the turbine and compressor blade surfaces would be accomplished using compact exchange devices such as evaporative heat pipes. Thermal energy would be transferred from the hot section of the engine to the cold section. Using experimental data and the NTU formulas derived, the effectiveness of this integrated exchange system was found to be 4.5%.

## 3. Integrated Recuperation

The efficiency of the traditional regenerative cycle was computed assuming 100% effectiveness. The efficiency of the regenerative cycle using integrated recuperation with 4.5% effectiveness was computed and compared to that of the basic cycle. A ratio of efficiencies was computed and plotted against pressure ratio in Figure 22.

$$efficiency\_ratio = \frac{\eta_{integrated\_recuperation}}{\eta_{basic\_cycle}}$$
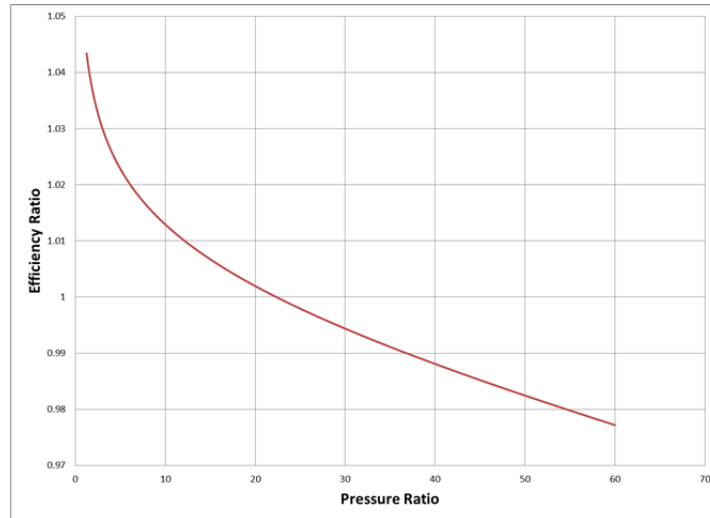


Figure 22.    Ratio of Integrated Recuperation Efficiency to
Basic Brayton Efficiency

The efficiencies of the two cycles are equal at an approximate pressure ratio of 22, where the efficiency ratio is equal to one. At the lowest pressure ratios efficiency of the integrated regenerative cycle is about 4.3% higher than the basic Brayton cycle. At higher pressure ratios, however, this integrated cycle is 2% less efficient than the basic cycle. Recuperation, integrated or otherwise, has no effect on the amount of power produced.

### 4.    Integrated Intercooling

An integrated heat exchange system can also be used to produce an intercooled cycle by removing heat and gradually cooling the flow as it is compressed. The efficiency of this intercooled cycle using the integrated heat exchange with 4.5% effectiveness was computed and compared to that of the basic cycle. A ratio of these efficiencies was computed and plotted against pressure ratio in Figure 23.

$$efficiency\_ratio = \frac{\eta_{integrated\_intercooling}}{\eta_{basic\_cycle}}$$
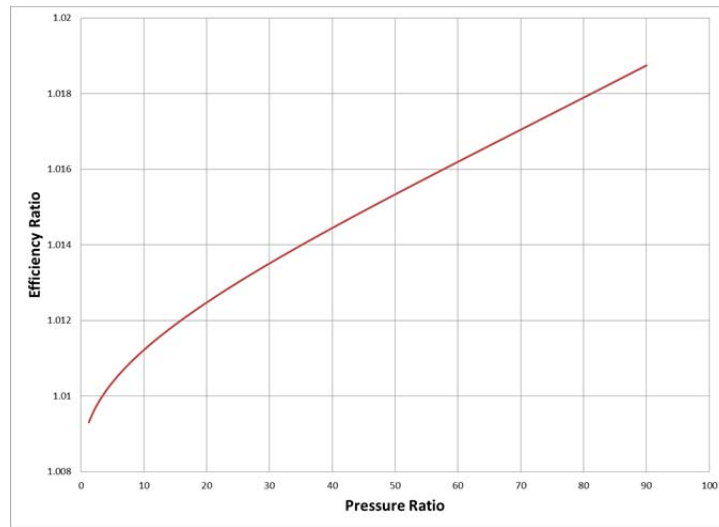


Figure 23.    Ratio of Integrated Intercooling Efficiency to
Basic Brayton Efficiency

The integrated intercooling system improves efficiency across the entire range of pressure ratios. At the lowest pressure ratios efficiency is improved by 1%. At the highest pressure ratios efficiency is approximately 2% greater than the basic cycle.

The specific power of this intercooled cycle using the integrated heat exchange with 4.5% effectiveness was also computed and compared to that of the basic cycle. A ratio of these specific powers was computed and plotted against pressure ratio in Figure 24.

$$power\_ratio = \frac{w_{net\_integrated\_cooling}}{w_{net\_basic\_cycle}}$$
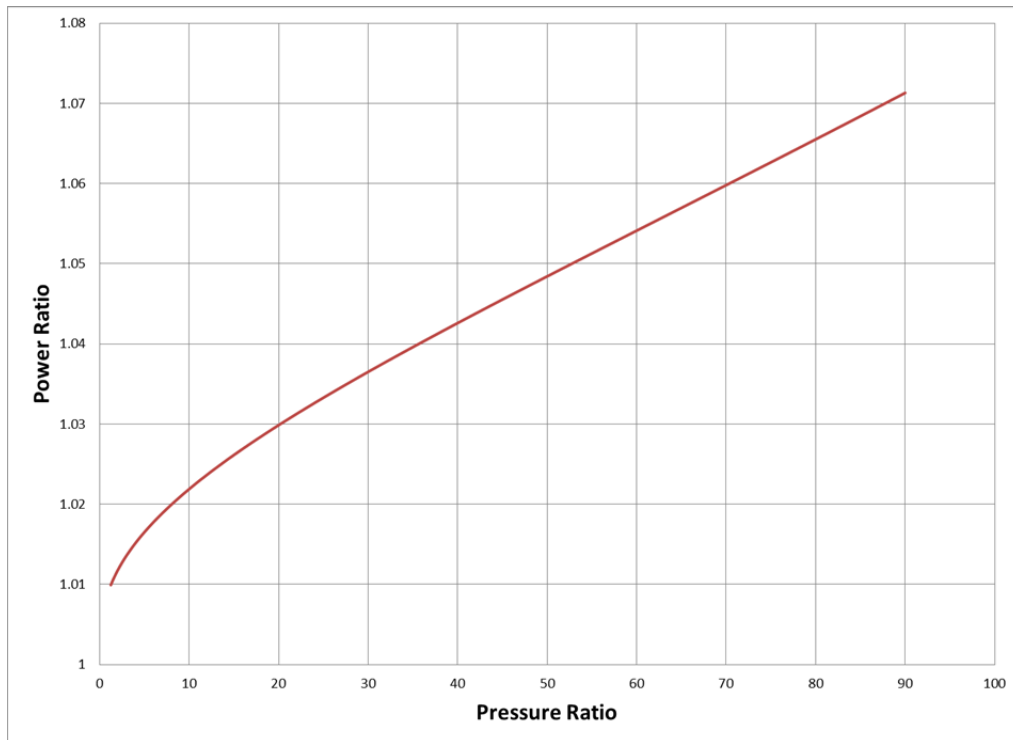


Figure 24.  Ratio of Integrated Cooling Cycle Power to
Basic Brayton Cycle Power

The net power output of the integrated cooling cycle is also greater than that of the basic cycle. Integrated intercooling increases the power output by 1% for the lowest pressure ratios and 7% at higher pressure ratios.

## B.    CONCLUSIONS

The common Brayton cycle modifications presented in this study offer potential improvements in fuel efficiency that are worth investigating further.  These modifications require the addition of large engine components such as regenerators or intercoolers.  Thus, this technology is only feasible in land-based engines.  Transferring this technology to aviation or ship engines is difficult due to the size and weight constraints associated with these vehicles.  A proposed solution is to embed a heat exchange system within the engine using existing blade surfaces to transfer heat via evaporative heat pipes.

Due to the highly turbulent and transient flow, heat transfer coefficients in turbomachinery are extremely high, making it possible to embed this integrated heat exchange system with in the engine.  The resulting 4.5% heat exchange effectiveness of this system indicates that this approach is feasible.  Effectiveness of this system in a real engine would likely be higher as conductivities are higher at higher gas temperatures.  Integrated heat exchange can be used for recuperation and intercooling within an engine cycle.

Integrated recuperation improves thermal efficiency at compressor pressure ratios less than 22.  The LM2500 Marine Gas Turbine is an engine manufactured by General Electric and used aboard USN cruisers and destroyers.  It operates with 36% thermal efficiency and utilizes a 16-stage compressor with a pressure ratio of 18 [22].   The efficiency increase resulting from integrated recuperation at an 18:1 pressure ratio is about 0.3%.  Integrated intercooling improves efficiency by 1.2% and power output by about 2.8% at a pressure ratio of 18.

These minor performance gains may seem insignificant but a 1–2% increase in the fuel efficiency of a single engine can save significant amounts of fuel and increase range and endurance; adding significantly less weight than a recuperator or intercooler.

## C.    FUTURE WORK AND RECOMMENDATIONS

### 1.    Intercooled Recuperation via Integrated Heat Exchange

The next step is to determine the feasibility of applying this technology to the concept of combined intercooled recuperation and comparing the performance gains to that of the WR-21 gas turbine engine.

### 2.    Evaporative Heat Pipes

Unlike most heat transfer systems, the integrated heat exchange system presented in this study is based on the idea of phase change; phase change within evaporative heat pipes.  It is necessary to determine how to practically embed these heat pipes in existing engines and what impact such an addition will have on the performance of the engine.

### 3.    System Optimization

Research should be done in how to effectively optimize the integrated heat transfer system.  Increasing blade size and surface area should be considered in order to maximize the amount of heat transferred.  In this study, it was assumed that the area of the engine hot section was equal to that the cold section.  Consideration should be made in varying these areas.

### 4.    Hybrid Heat Exchange System

Heat transfer via phase change and heat pipes is the smallest scale of recuperation with 4.5% effectiveness.  Heat transfer and recuperation via heat exchangers and intercoolers is the largest scale at an effectiveness of 50%–60%.  Exploration into the possibility of a hybrid heat exchange system consisting of a heat pipe network and perhaps a small heat exchanger.  This may result in a heat exchange effectiveness less than 50% but could be significantly greater than the 4.5% effectiveness of the heat piped system alone.

Heat transfer in gas turbine engines via phase change is a relatively new concept. The USN and USMC will benefit greatly from further research in this area.

# LIST OF REFERENCES

[1]     "Strategy for Renewable Energy." 2012, United States Department of the Navy, Washington, DC.

[2]     Crisalll, A. J. and Parker, M. L., 1993, "Overview of the WR-21 Intercooler Recuperated Gas Turbine Engine System, a Modern Engine for a Modern Fleet," *International Gas Turbine and Aeroengine Congress and Exposition*, 1993.

[3]     Crichton, T., 2016, "Royal Navy in Hot Water as Engines of Britain's Flagship Destroyers Breakdown in Middle of Sea," Daily Record, from http://www.dailyrecord.co.uk/news/uk-world-news/royal-navy-hot-water-engines-8128618

[4]     Macdonell, B., McDonough, P., Boral, K., and Fukuizumi, Y., 2005 "Operational Esperience of MHI G Series Steam Cooled Gas Turbine in the USA" *POWER-GEN International 2005*.

[5]     Shah, P. and Tan, C., 2007, "Effect of Blade Passage Surface Heat Extraction on Axial Compressor Performance," *Journal of Turbomachinery*, **129**, pp. 457–467.

[6]     Bruna, D. and Turner, M. G., 2013, "A Rothalpy Analysis for the Isothermal Boundary Condition at Casing Applied to the Rotor 37 Transonic Axial Flow Compressor," *ASME Turbo Expo 2013: Turbine Technical Conference Exposition.*

[7]     Gannon, A. and Hobson, G., 2015, "Measured Heat Transfer in a Transonic Fan Rig at Casing with Implications on Performance," *ASME Turbo Expo 2015*.

[8]     Gannon, A., Turner, M., and Sanz, W., 2015, "Performance of a Splittered Transonic Rotor with Several Tip Clearances," *ASME Turbo Expo 2015*.

[9]     Korn, F., 2008, *Heat Pipes and its Applications*, Lund University, Sweden.

[10]    Kew, P. and Reay, D., 2006, *Heat Pipes: Theory Design and Applications,* New York, Elsevier Science.

[11]    AAVID THERMALLOY, 2016, "How a Heat Pipe Works," from http://www.aavid.com/product-group/heatpipe/operate.

[12]    Dunn, P. and Reay, D., 1993, *Heat Pipes,* New York, Elsevier Science.

[13]    Advanced Thermal Solutions Inc., 2016, "Advance Thermal Solutions," from http://www.qats.com/Products/Heat-Pipes.

[14]   Ye, L., Tong, Z., Huang, L. and Chen, H., *Studies on Heat Transfer Performances of a Heat Pipe Radiator Used in Desktop PC for CPU Cooling*, Shanghai, IOP Publishing.

[15]   Saha, U.K., *Internal Combustion Engines: Engine Heat Transfer*, Guwahati, Indian Institute of Technology.

[16]   Borgnakke, C. and Sonntag, R. E., 2009, *Fundamentals of Thermodynamics*, John Wiley and Sons, Hoboken, NJ.

[17]   *Airplane Flying Handbook*, 2004, US Department of Transportation Federal Aviation Administration, Washington, DC.

[18]   Cumpsty, N., 2005, *Jet Propulsion*, 2nd ed., Cambridge University Press, Cambridge

[19]   Huang, M. and Gramoll, K., "eCourses: Thermodynamics," from https://ecourses.ou.edu/cgi-bin/ebook.cgi?topic=th.

[20]   Incropera, F. P., Dewitt, D. P., Bergman, T. L. and Lavine, A. S., 2007, *Fundamentals of Heat and Mass Transfer*, John Wiley and Sons, Danvers, MA.

[21]   "Integrated Publishing,"  TM-55-2840-251-23_219, from http://aviationmiscmanuals.tpub.com/TM-55-2840-251-23/css/TM-55-2840-251-23_219.htm

[22]   General Electric, 2016, "GE Aviation," from http://www.geaviation.com/engines/docs/marine/datasheet-lm2500.pdf

# INITIAL DISTRIBUTION LIST

1. Defense Technical Information Center
   Ft. Belvoir, Virginia

2. Dudley Knox Library
   Naval Postgraduate School
   Monterey, California